ChemPubSoc Europe

DOI: 10.1002/chem.201602573

CHEMISTRY
A European Journal
Full Paper

Tautomer Reactivity

The Importance of Methyl Positioning and Tautomeric Equilibria for Imidazole Nucleophilicity

Renan B. Campos,[a, b, c] Leociley R. A. Menezes,[a] Andersson Barison,[a] Dean J. Tantillo,[b] and Elisa S. Orth*[a]

Abstract: Imidazole (IMZ) rings catalyze many biological dephosphorylation processes. The methyl positioning effect on IMZs reactivity has long intrigued scientists and its full understanding comprises a promising tool for designing highly efficient IMZ-based catalysts. We evaluated all monosubstituted methylimidazoles (xMEI) in the reaction with diethyl 2,4-dinitrophenyl phosphate by kinetics studies, NMR analysis and DFT calculations. All xMEI showed remarkable rate enhancements, up to 1.9×10^5 fold, compared with spontaneous hydrolysis. Unexpectedly, the electron-donating methyl group acts to decrease the reactivity of the xMEI compared to IMZ, except for 4(5)methylimidazole, (4(5)MEI). This behavior was attributed to both electronic and steric effects. Moreover, reaction intermediates were monitored by NMR and surprisingly, the reactivity of the two different 4(5)MEI tautomers was distinguished.

Introduction

Phosphate esters are known for their high P–O bond stability (e. g., resistance to hydrolysis), hence they exert multiple vital biological roles.[1] In contrast, phosphotriesters are typically toxic, and in environmental conditions leads to bioaccumulation, which in turn is a serious concern in the development of lethal substances like pesticides, insecticides and even chemical weapons.[2] Worldwide, the growth of food production has been followed by a disproportionate increase in the use of agrochemicals. For example, Brazil has become the greatest consumer of pesticides in the world, and alarmingly, uses some products that have been already banned elsewhere.[3] Therefore, the search of new and efficient catalysts that target the detoxification of organophosphorus pesticides (OPP) with the potential to destroy large unused stocks (mostly prohibited) and also for monitoring abusive amounts of OPP in the environment and food, is assuredly important.

Consequently, mechanistic investigations on dephosphorylation have attracted increasing interest, especially those involving the design of optimum molecular architectures for catalyzing dephosphorylation. In this context, imidazole (IMZ) is a promising starting scaffold for developing catalysts, since its pK_a of approximately 7 guarantees acidic, basic and nucleophilic properties. Present in the histidine residue, IMZ plays essential roles in biological reactions involving phosphoryl group transfer, such as the cleavage of RNA and signaling processes, with the formation of phosphohistidines.[4] Interestingly, the biological versatility and effectiveness of this group has justified pharmacological activities of some IMZ derivatives, yielding the development of many drugs including antifungals, antibiotics, antiseptics and even antineoplastics.[5] Nonetheless, since the catalytic activity of IMZ in organisms is not fully understood, mutagenesis and other collateral effects may be linked with the extended use of medicines from this class of compounds.[6] Therefore, studies aimed at the elucidation of detailed reaction mechanisms involving IMZ derivatives and phosphate esters may provide not just support for organism-drug interactions research, but also for the development of novel and efficient catalysts for detoxification.

Among IMZ derivatives, the monosubstituted methylimidazoles (xMEI) stand out since, despite their simple structures, their reactivity has not been concisely correlated with methyl positioning for various reactions (e.g. dephosphorylation, deacylation).[7] Indeed, the effects of methyl substitution have intrigued scientists for several years. Scheme 1 presents all xMEI derivatives: 1-methylimidazole (1 MEI), 4(5)-methylimidazole (4(5)MEI) and 2-methylimidazole (2 MEI). The known tautomeric equilibrium in aqueous solution for IMZ is also present in 2 MEI and 4(5)MEI. However, due to symmetry, although for IMZ and 2 MEI this effect results in an equilibrium between two species with the same structure, for 4(5)MEI it involves two different species: 4 MEI and 5 MEI.[8] 4(5)MEI tautomers should have different properties, such as reactivity, and determining these is focus of our study.

[a] R. B. Campos, L. R. A. Menezes, Prof. Dr. A. Barison, Prof. Dr. E. S. Orth
Department of Chemistry, Universidade Federal do Paraná
CP 19081, CEP 81531-990; Curitiba-PR (Brasil)
E-mail: elisaorth@ufpr.br

[b] R. B. Campos, Prof. Dr. D. J. Tantillo
Department of Chemistry, University of California-Davis
Davis, California 95616 (USA)

[c] R. B. Campos
current address: Departamento Acadêmico de Química e Biologia
Universidade Tecnológica Federal do Paraná
Curitiba, PR, ZIP 81280-340 (Brazil)

Supporting information for this article is available on the WWW under http://dx.doi.org/10.1002/chem.201602573.

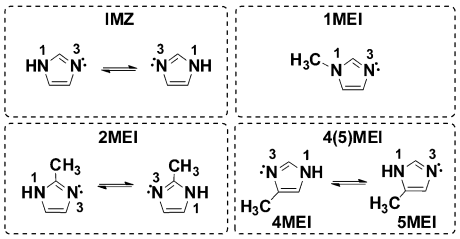

Scheme 1. xMEI structures and tautomeric equilibria.

It is important to highlight that the mechanistic understanding for dephosphorylation reactions with IMZ derivatives is sometimes limited by the fact that the P–N bond is highly unstable,[4a] making intermediates difficult to monitor. Consequently, the combination of experimental and computational studies has allowed new insights into these processes.[7i,9] Herein, we present mechanistic insight into the reactions of 1 MEI, 2 MEI and 4(5)MEI with diethyl 2,4-dinitrophenylphosphate (DEDNPP) in aqueous solution, based on various experimental techniques: kinetics, 1D/2D nuclear magnetic resonance (^{1}H, ^{13}C, ^{31}P NMR) and theoretical calculations. Surprisingly, phosphorylated intermediates for the 4(5)MEI tautomers were distinguished by NMR. Furthermore, a comprehensive theoretical study was carried out that sheds light on the mechanisms involved and the main factors that govern the relative reactivity of xMEI species.

Results and Discussion

Kinetics

All xMEI showed remarkable catalytic activity in the dephosphorylation of DEDNPP, as depicted in the pH rate profiles shown in Figure 1. The expected dependence of k_{obs} with pH is observed, confirming the reactivity of the neutral nucleophilic species (plateau around the pK_a). The fitting of experimental results, given by the solid lines in Figure 1, is based on Equation 1, in which the terms correspond to the contribution of hydrolysis (k_0), alkaline hydrolysis (k_{OH}) and xMEI reactions (k_N),

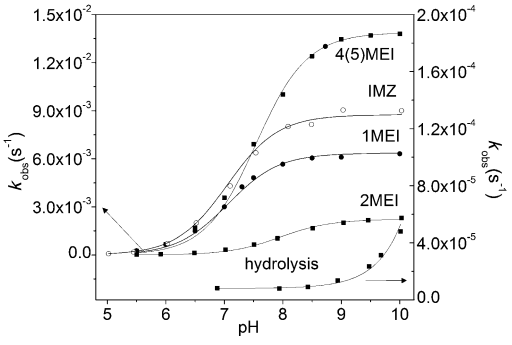

Figure 1. pH rate profiles for the reactions of xMEI and IMZ with DEDNPP, 0.5 M at 25 °C (left axis). The spontaneous hydrolysis of DEDNPP (right axis) and the IMZ profile are shown for comparisons.[4a] The fitting (solid lines) are based on Equation 1.

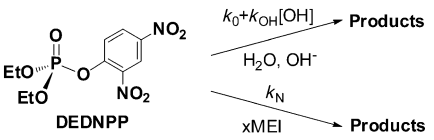

Scheme 2. Proposed pathways for the reactions of DEDNPP with xMEI studied herein.

Table 1. Kinetic parameters for the reaction of xMEI and IMZ with DEDNPP.[a]

	4(5)MEI	IMZ[4a]	1 MEI	2 MEI
k_0 [s^{-1}]	8.0×10^{-6}			
k_{OH} [$M^{-1}s^{-1}$]	0.25			
k_N [$10^{-3}M^{-1}s^{-1}$]	27.7 (0.29)	17.7 (0.21)	12.8 (0.09)	4.4 (0.08)
pK_a[11]	7.69	6.95	7.21	7.85

[a] Experimental data, equations and plots are given in the Supporting Information. Errors are given in round parentheses.

respectively (Scheme 2). The term χ_{xMEI} refers to the molar fraction of the neutral reactive species of each xMEI. Kinetic parameters are presented in Table 1.

$$k_{obs} = k_0 + k_{OH}[OH^-] + k_N[xMEI]\chi_{xMEI} \quad (1)$$

The results show rate enhancements of 1.9×10^5, 8.9×10^4 and 3.0×10^4 for 4(5)MEI, 1 MEI and 2 MEI, respectively, compared to the spontaneous hydrolysis of the triester. Interestingly, this reactivity trend is not directly related to the xMEI pK_a values (for protonated species), shown in Table 1. In fact, 2 MEI shows the lowest reaction rate compared to all derivatives, in contrast to the highest pK_a value, which would normally suggest a more reactive nucleophile.[10] Finally, the most effective catalyst for the cleavage of DEDNPP is 4(5)MEI, showing experimental k_N values 1.6-, 2.2- and 6.3-fold higher than IMZ, 1 MEI and 2 MEI, respectively.

To help assess the reaction pathway and to provide comparisons for calculations, thermodynamic parameters were obtained (Table 2) through Eyring plots (given in the Supporting Information). The largely negative values of entropies of activation obtained indicate that the reaction mechanism for all cases is in fact most likely a bimolecular nucleophilic displacement pathway.[4a]

Table 2. Activation parameters for the reactions of xMEI and IMZ (pH 8.5) with DEDNPP.[a]

Cmpd.	$\Delta H^{\neq}$ [kcal.mol^{-1}]	$\Delta S^{\neq}$ [cal.K^{-1}mol^{-1}]	$\Delta G^{\neq}$ [kcal.mol^{-1}]
4(5)MEI	7.4	−42.7	20.1
2 MEI	9.0	−41.2	21.2
1 MEI[12]	9.6	−37.0	20.6
IMZ[12]	7.7	−42.6	20.4

[a] Experimental data, equations and plots are given in the Supporting Information.

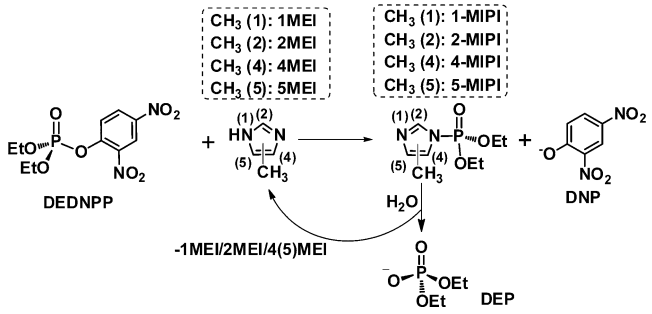

Scheme 3. Mechanistic proposal for the dephosphorylation of DEDNPP in which the intermediates labels (1 to 5-MIPI) are based on methyl positioning in xMEI. The second step illustrates that xMEI are regenerated after the xMIPI hydrolysis.

The rate enhancements and activation parameters observed for the methyl nucleophiles are typical of nucleophilic attack and, based on previous studies,[4a,12] we propose the mechanism presented in Scheme 3, in which the nitrogen lone pair of xMEI attacks the phosphorous atom of DEDNPP and displaces 2,4-dinitrophenolate (DNP, $pK_a = 4.1$)[11] through a concerted mechanism, leading to a phosphorylated intermediate that should easily hydrolyze, regenerating the nucleophile.[13] It is important to note that UV/Vis kinetic study follows the appearance of DNP, hence, k_N in Table 1, refers solely to the first step of the mechanism. The decomposition of the phosphorylated intermediates is expected to be fast, since they are knowingly unstable.[4b] As will be discussed in following sections, NMR analysis combined with DFT calculations support this overall hypothesis and also provide important information on methyl positioning effects on the reaction rates, not straightforward by UV/Vis studies.

Mechanistic investigation by NMR

For a more detailed mechanistic understanding, reactions of DEDNPP with 2 MEI and 4(5)MEI (NMR data for IMZ and 1 MEI has been reported previously)[4a,12] were investigated through ^{1}H and ^{31}P{^{1}H} NMR spectroscopy. Indeed, a thorough analysis of 1D NMR spectra and 2D NMR correlation maps lead to the complete ^{1}H, ^{13}C, and ^{31}P NMR chemical shift assignments given in Table 3, Figures 2 and 3 and in the Supporting Information, which are consistent with Scheme 3. Firstly, for the reaction of DEDNPP with 2 MEI, ^{31}P{^{1}H} NMR spectra showed the peaks at −7.5 and 0.8 ppm assigned to DEDNPP and diethylphosphate (DEP), respectively, and an additional signal at −4.9 ppm (Figure 2 and Scheme 3). Moreover, ^{1}H NMR spectra showed an additional set of signals, including a spin system at 7.32 and 7.02 ppm, as well as a signal at 2.53 ppm from a methyl group, that were different than those observed for 2 MEI (Table 3). An additional spin system also was observed for ethoxy groups at 3.92 and 1.25 ppm in the ^{1}H NMR spectrum, different than initially observed for DEDNPP (Table 3). All these hydrogen showed ^{1}H–^{31}P long-range NMR correlation with the same phosphorous species at −4.9 ppm, supporting the structure of the intermediate 2-MIPI (Scheme 3). Additionally, a second aromatic spin system emerged in the ^{1}H NMR spectra during the course of reaction, with no ^{1}H–^{31}P long-range NMR correlation, that were assigned to the phenolic product DNP (Scheme 3, Table 3).

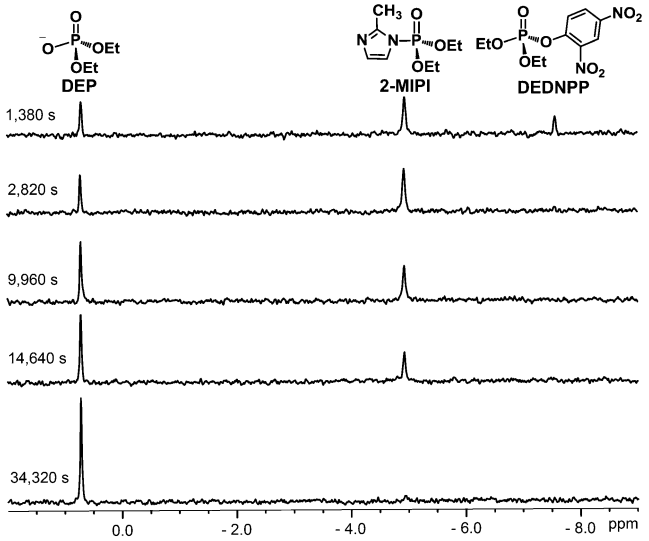

Figure 2. ^{31}P{^{1}H} NMR spectra for the reaction of DEDNPP (7.5×10^{-3} M) with 2 MEI (0.3 M), pH 8.5, 25 °C.

The ^{31}P{^{1}H} NMR spectra sequentially acquired directly from the reaction medium with 2 MEI, Figure 2, showed the signal at −7.5 ppm from DEDNPP decreasing and the simultaneous increase of the signal at 0.8 ppm from DEP, according to reac-

Table 3. NMR data (600 MHz, H_2O/D_2O at pH 8.5 and 25 °C)[a] for the species detected in the reaction of DEDNPP with 2 MEI and 4(5)MEI.[b]

Cmpd.	δ_H	δ_P
2 MEI	7.09 (s, 2H, Ar), 2.45 (s, 3H, CH_3)	
4(5)MEI	7.80 (s, 1H, Ar), 6.87 (q, 1H, Ar), 2.23 (d, 3H, CH_3)	
DEDNPP	8.99 (dd, 1H, Ar), 8.63 (dd, 1H, Ar), 7.80 (dd, 1H, Ar), 4.38 (dq, 4H, CH_2), 1.39 (td, 6H, CH_3)	−7.5
2-MIPI	7.32 (d, 1H, Ar), 7.02 (d, 1H, Ar), 4.27 (dq, 4H, CH_2), 2.53 (s, 3H, CH_3), 1.35 (td, 6H, CH_3)	−4.9
4-MIPI	7.83 (Ar)[c], 6.88 (Ar)[c], 4.25 (dq, 4H, CH_2), 2.33 (d, 3H, CH_3), 1.33 (td, 6H, CH_3)	−5.2
5-MIPI	7.91 (s, 1H, Ar), 7.05 (q, 1H, Ar), 4.22 (dq, 4H, CH_2), 2.20 (d, 3H, CH_3), 1.32 (td, 6H, CH_3)	−5.6
DNP	8.85 (dd, 1H, Ar), 8.09 (dd, 1H, Ar), 6.74 (dd, 1H, Ar)	
DEP	3.92 (dq, 4H, CH_2), 1.25 (td, 6H, CH_3)	0.8

[a] Additional data given in the Supporting Information. [b] The assignments for DEDNPP, DNP and DEP are in agreement with data found in the literature.[4a,12] [c] Overlapping signal.

tion progress. As expected, the signal at −4.9 ppm decreases and disappears as the phosphorylated intermediate is hydrolyzed.

Surprisingly, for the reaction of DEDNPP with 4(5)MEI, $^{31}P\{^{1}H\}$ NMR spectra showed two new signals (−5.2 and −5.6 ppm) in addition to those for DEDNPP and DEP (Figure 3 and Table 2). This indicates two phosphorylated intermediates, which were attributed to separate reactions of the tautomers 4 MEI and 5 MEI (Scheme 3). The ^{1}H NMR spectra also showed

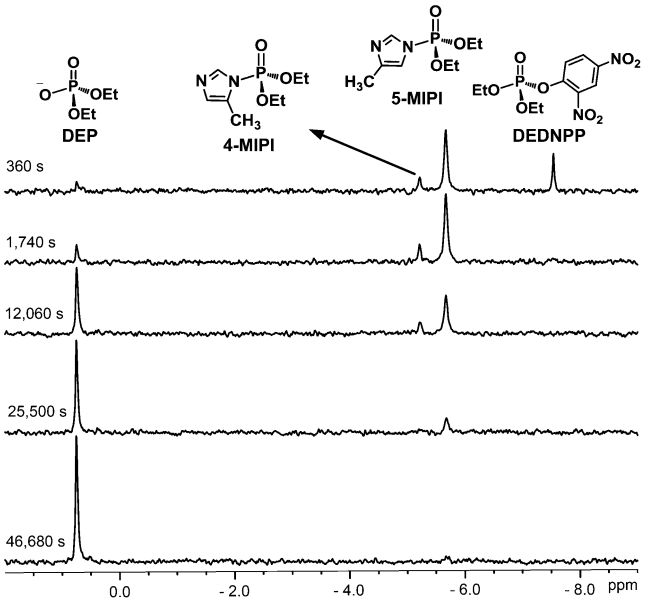

Figure 3. $^{31}P\{^{1}H\}$ NMR spectra for the reaction of DEDNPP (7.5×10^{-3} M) with 4(5)MEI (0.04 M), pH 8.5, 25 °C.

two additional sets of signals. The first set of hydrogen nuclei at 7.91, 7.05 and 2.20 ppm from the IMZ moiety and those at 4.22 and 1.32 ppm from ethoxy moieties showed ^{1}H–^{31}P long-range NMR correlation with the same phosphorous species at −5.6 ppm. The second set of hydrogen nuclei at 7.83, 6.88 and 2.33 ppm from the IMZ moiety and those at 4.25 and 1.33 ppm from ethoxy moieties showed ^{1}H–^{31}P long-range NMR correlation with the same phosphorous species at −5.2 ppm. In addition, DNP signals again were observed in the ^{1}H NMR spectra.

Consecutive $^{31}P\{^{1}H\}$ NMR spectra for the reaction of DEDNPP with 4(5)MEI evidenced the consumption of DEDNPP and formation of DEP (Figure 3), as observed previously. Simultaneously, the signals at −5.2 and −5.6 ppm from 4-MIPI and 5-MIPI showed the typical increase followed by a decrease, with the latter showing higher stability (i.e. a longer lifetime). Distinction of these phosphorylated isomers is a benchmark for understanding overall reactivity of IMZ derivatives and their stability was accessed by further kinetic analysis (vide infra).

Seeking a deeper understanding, kinetic profiles from the ^{31}P NMR data were obtained and are shown in Figure 4. Rate constants relative to the formation and hydrolysis of the intermediates were calculated by fitting the profiles of relative concentration versus time with equations for consecutive first-order reactions,[4a] and the results are summarized in Table 4.

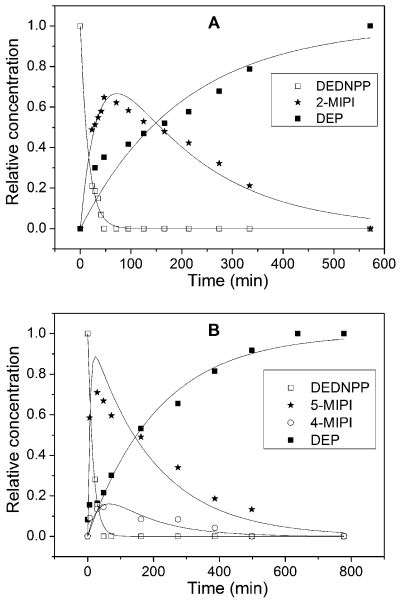

Figure 4. Relative concentration vs time kinetic profiles for the species involved in reactions of (A) 2 MEI and (B) 4(5)MEI with DEDNPP, detected by ^{31}P NMR at 25 °C, according to Scheme 3. Residual plots are given in the Supporting Information.

Analysis of the data in Table 4 shows a reactivity trend for the nucleophiles in agreement with the UV/Vis kinetic study previously shown, hence 4(5)MEI > 2 MEI. Thus, the reactivity of 4(5)MEI tautomers could be evaluated solely by ^{31}P NMR kinetic. 5 MEI shows higher reactivity than 4 MEI (31-fold) that cannot be associated simply to the tautomer population distribution. Indeed, the Boltzmann distribution from previously reported computational results for 4(5)MEI, indicates a 40:60 ratio of 5 MEI/4 MEI (Scheme 1);[8] thus, the 4(5)MEI reaction fits with a Curtin–Hammett scheme. In fact, 4 MEI showed only

Table 4. Rate constants of formation (k_1), cleavage (k_2) and half-life of the intermediates involved in reaction of 2 MEI and 4(5)MEI with DEDNPP, obtained by fitting data in Figure 4.[a]

Intermediate	k_1 [$M^{-1}s^{-1}$]	k_2 [s^{-1}]	Half-life [s]
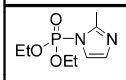 4-MIPI	15.2×10^{-3} ($\pm2.58\times10^{-3}$)	6.33×10^{-4} ($\pm1.11\times10^{-4}$)	1500
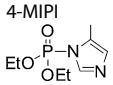 2-MIPI	8.17×10^{-3} ($\pm4.08\times10^{-4}$)	9.35×10^{-5} ($\pm4.77\times10^{-6}$)	7380
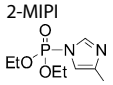 5-MIPI	0.47 ($\pm$0.127)	8.63×10^{-5} ($\pm1.25\times10^{-5}$)	7980

[a] Fitting was based on consecutive first-order reaction equations.[4a] Errors are given in round parentheses.

a marginally higher reactivity than 2 MEI (Table 4), which in turn presents the lowest nucleophilicity toward the triester.

The relative stability of the phosphorylated intermediates (Figure 4 and k_2 in Table 4) can be attributed to their leaving group (xMEI) basicity, however the pK_a of protonated 4(5)MEI (7.69)[11] is weighted by the contribution of both tautomers 5 MEI and 4 MEI and a direct analysis is not straightforward. Nonetheless, the gas phase proton affinity is a reasonable approach to estimate basicity of a compound and, in fact, it is predicted (vide infra) to be slightly (0.6 kcal mol^{-1}) higher for 5 MEI than for 4 MEI.[14] Although this difference is small, it is in agreement with the lower lifetime of 4-MIPI relative to 5-MIPI since it is expected that 4 MEI is a better leaving group. It is important to note the solvent composition of the reaction medium for NMR kinetic studies: 46 and 10% (in volume) of acetonitrile and D_2O, different from UV/Vis study. This large amount of acetonitrile should affect more significantly k_2, slowing down this process.[15] Although it is important to assess the half-life of the intermediates, the analysis herein are valid solely under these conditions of solvents. Overall, the most important observation obtained from the NMR study is to confirm the intermediate structure. The kinetic profiles are shown to complement the study but caution should be taken when analyzing it. Firstly, the solvent composition is important and secondly the apparent build-up of the intermediates is in terms of relative concentration of the species detected by ^{31}P NMR, hence, only phosphorylated species. If we consider the DNP product, which was not detected by ^{31}P NMR, this built-up would not be as much (lower concentration).

It is noteworthy that we already reported similar NMR kinetics for the reactions of DEDNPP with IMZ and 1 MEI,[4a,12] for which an analogous behavior was observed involving the formation of phosphorylated intermediates. As pointed out previously, detection and most importantly understanding the reactivity of IMZ-based phosphorylated intermediates is fundamental for biological purposes[4a] and we hope that the full set NMR assignments and kinetic for the xMEI-based intermediates presented furnishes an important database for future studies.

Undoubtedly, mechanistic investigation by NMR analysis was crucial for confirming the proposed catalyzed nucleophilic reaction between xMEI and DEDNPP (Scheme 3), and complements UV/Vis kinetic data. Additionally, discerning reactivity of the tautomers 4 MEI and 5 MEI was possible, which is interesting from the mechanistic point of view and will hopefully inspire further detailed studies involving nucleophiles with tautomers. Nonetheless, in order to fully understand the methyl positioning effect for IMZ derivatives, as well as to probe whether the substitution reactions occur via concerted or stepwise mechanisms, DFT calculations were pursued.

DFT calculations for understanding the reaction mechanism and the methyl positioning effect

Our experimental results show that the effect of a methyl group at most positions of the IMZ ring decreases its nucleophilicity towards DEDNPP, when compared to unsubstituted IMZ. However, in the absence of steric effects, it is generally expected that the presence of this substituent acts to enhance the nucleophilicity of a molecule due to hyperconjugative donation. The reactivity of 2 MEI towards DEDNPP is lower than IMZ, 1 MEI and 4(5)MEI, indicating that a steric effect involving the methyl group close to the nucleophilic nitrogen atom likely inhibits nucleophilic attack on phosphorus. In rationalizing the higher reactivity of 4(5)MEI, it is important to note that, in contrast to 1 MEI, the positioning of the methyl group in 2 MEI and 4(5)MEI allows its tautomerism, thus, reaction can occur on both nitrogen atoms. For 2 MEI, these tautomers are identical, but for 4(5)MEI, NMR results herein clearly show different reactivity for the 4 MEI and 5 MEI tautomers. Indeed, the reactivities of 2 MEI and 4 MEI are similar (k_1 in Table 4), which is expected due to their similar steric hindrance—both have a methyl group α to the nitrogen atom. Hence, the 5 MEI tautomer is responsible for the increased effectiveness of 4(5)MEI in the dephosphorylation reaction. DFT calculations were carried out to explore these effects.

Firstly, we carried out calculations with the M06-2X[16] and B3LYP[17] functionals combined with the 6-31+G(d,p) and 6-311++G(d,p) basis sets to ascertain which method/basis set provides $\Delta G^{\neq}$ values in accord with the experimentally observed reactivity trend. Unexpectedly, B3LYP calculations with the smaller basis set best reproduced the experimental reactivity trend, 5 MEI > IMZ > 1 MEI > 4 MEI ≈ 2 MEI, although barrier heights were overestimated with this level of theory (Figure 5). The same functional with a larger basis set 6-311++G(d,p) predicted reversed barriers for 1 MEI and IMZ, whereas M06-2X/6-31+G(d,p) predicted that IMZ is the best nucleophile in the dephosphorylation reaction. When M06-2X is combined with a larger basis set, 2 MEI actually is predicted to be the more reactive derivative (which is the least reactive according to experimental data; Figure 1), but furnishes a correct trend for the other nucleophiles.[18] Thus, all further discussions are focused on B3LYP/6-31+G(d,p) results. Relevant transition state structures (TSS) for the xMEI reactions, obtained with B3LYP/6-31+G(d,p), are shown in Figure 6, and activation barriers and selected geometrical parameters are presented in Table 5, Table 6 and Figure 7.

Although most geometric parameters of the TSSs do not vary much, the C6-N5-P-O2 dihedral angle varies significantly and tracks with the reaction barriers. For the less reactive nucleophiles (2 MEI and 4 MEI) these dihedral angles are close to

Table 5. Activation barriers (experimental and theoretical ($\Delta G^{\neq}$/kcal. mol^{-1}), HOMO energy (nucleophiles) and imaginary frequencies of the TSS for the reactions of xMEI and IMZ with DEDNPP.[a]

Cmpd.	Experimental	B3LYP 6-31+G(d,p)	TS imaginary frequency (cm^{-1})	E_{HOMO}[c] (Hartrees)
2 MEI	21.3	26.4	−135.071	−0.2276
1 MEI	20.6	24.2	−138.317	−0.2349
IMZ	20.4	24.0	−143.307	−0.2377
5 MEI	20.1[b]	23.3	−138.358	−0.2264
4 MEI	20.1[b]	26.3	−134.034	−0.2275

[a] Experimental data with xMEI 0.5 M, pH 8.5, 25 °C. [b] 4(5)MEI. [c] Obtained performing B3LYP/6-31+G(d,p) optimization.

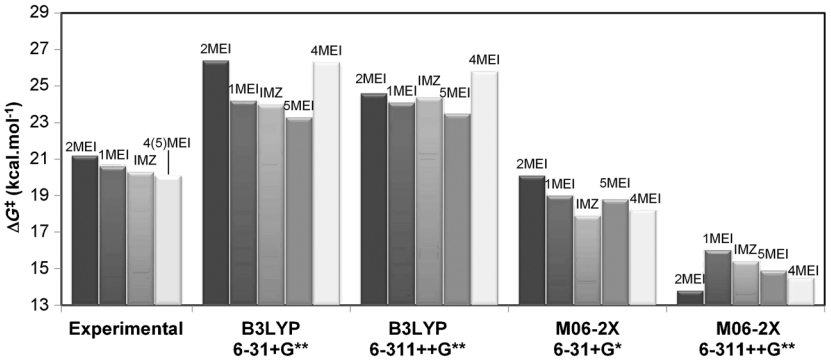

Figure 5. Experimental and calculated barriers $\Delta G^{\neq}$ (kcal mol^{-1}) for the reaction of xMEI and IMZ with DEDNPP. The experimental data were obtained from Eyring plots as given at the Supporting Information.

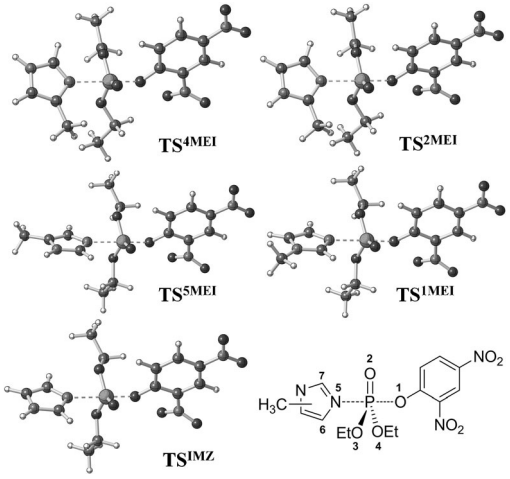

Figure 6. $S_N2(P)$ transition states for the reaction of xMEI and IMZ with DEDNPP obtained with B3LYP/6-31G + (d,p) and the general labelled TSS. All Cartesian coordinates are given in the Supporting Information.

Table 6. Structural parameters[a,b] of the species involved in the reaction of xMEI and IMZ with DEDNPP as shown in Scheme 3.

Structure	N5-P[c]	P-O1[c]	C6-N5-P-O2[c]	H(C7)- O2
TS$^{2\,MEI}$	2.273	1.783	−56.75	–
TS$^{4\,MEI}$	2.260	1.787	−56.88	4.096
TS^{IMZ}	2.274	1.783	−21.13	2.734
TS$^{1\,MEI}$	2.274	1.782	−17.88	2.757
TS$^{5\,MEI}$	2.285	1.780	−12.10	2.737
DEDNPP	–	1.642	–	–
2-MIPI	1.754	–	37.70	–
4-MIPI	1.757	–	40.59	4.302
IPI[d]	1.755	–	15.67	2.747
1-MIPI	1.750	–	18.06	2.765
5-MIPI	1.752	–	13.39	2.725

[a] Additional data are given in the Supporting Information. [b] Obtained performing B3LYP/6-31 + G(d,p) calculations. [c] As labeled in Figure 6. [d] Phosphorylated intermediate formed with the non-substituted IMZ.

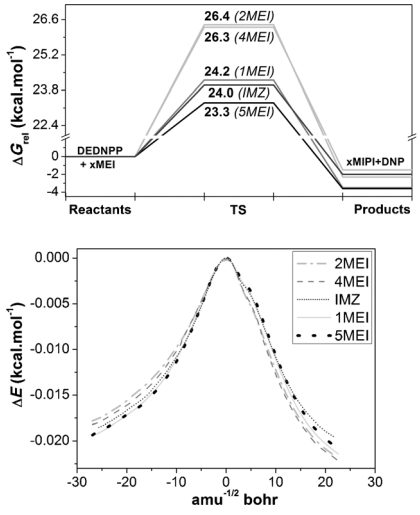

Figure 7. (A) Reaction coordinate diagram and (B) relative energies plots on the IRC calculated with B3LYP/6-31 + G(d,p).

−57°, whereas they are much lower for IMZ, 1 MEI and 5 MEI (−21, −18° and −12°, respectively). These results are consistent with the nucleophilic attack by 2 MEI and 4 MEI involving significant steric hindrance between the methyl group and the O2 atom, that is, the rotation minimizes this effect. As observed in the IRC plots shown in Figure 7, all reactions are concerted. Based on geometries, the formation of the N5–P bond and the cleavage of the P–O1 bond occur synchronously along the reaction coordinate.

Finally, since the nucleophiles 5 MEI and 1 MEI do not present steric hindrance from the methyl group, a different explanation for their reactivity difference is required. We note that differences in the HOMO energies for these species do correlate with reactivity, consistent with an electronic origin of the reactivity difference. DFT calculations at the B3LYP/6-31 + G(d,p) level on xMEI structures show that 5 MEI and 4 MEI have the highest energy HOMOs and IMZ and 1 MEI the lowest (Table 5). Although the differences in energy are small, they are consistent with the higher reactivity of 5 MEI compared to 1 MEI and IMZ toward DEDNPP. It is worth mentioning that even if the HOMO energy of 2 MEI indicates a higher reactivity compared to 1 MEI and IMZ, the steric effect is preponderant and governs the reaction rates.

Conclusion

Herein, dephosphorylation reactions involving methylated IMZ derivatives (xMEI) and DEDNPP were thoroughly investigated using a combination of experimental analysis and theoretical calculations. Consistently, the methyl positioning in the IMZ ring has direct influence on the reaction rates. Indeed, all xMEI presented remarkable increases in the rate of cleavage of DEDNPP ($>3.0\times10^4$-fold), compared to the spontaneous hydrolysis, with the following nucleophilicity trend: 4(5)MEI > IMZ > 1 MEI > 2 MEI. Interestingly, 4(5)MEI presented a higher reactivity than IMZ, which can be attributed to the presence of a pair of tautomers that react differently for 4(5)MEI, and NMR analysis combined with DFT calculations revealed that the 5 MEI dominates its catalytic activity. The experimental monitoring of the different isomers formed during the reactions with DEDNPP was crucial for understanding the methyl positioning effect. In addition, kinetics for the phosphorylated intermediates were followed by NMR and their half-lives were shown to be related to the basicity of the leaving group.

In addition, for DFT calculations, the predicted barriers for nucleophilic dephosphorylation reactions are sensitive to the type of functional/basis set, suggesting that caution should be taken when modeling similar reactions; the application of more than one type of calculation may be essential. The trend in calculated barriers at the B3LYP/6-31+G(d,p) level is in good agreement with experimental data for the systems studied here. Computed geometries are consistent with steric repulsion present in 2 MEI and 4 MEI, caused by the methyl group adjacent to the nitrogen lone pair, being the key factor in lowering their reactivity towards DEDNPP. In contrast, 5 MEI and 1 MEI are free of steric hindrance, allowing an electronic effect to increase the reactivity of 5 MEI (i.e., 5 MEI has a higher HOMO energy). Calculations also indicate concerted mechanisms with significant synchronism between bond making and forming events for all reactions studied.

Figure 8 summarizes the antagonistic methyl positioning effect for the reactions of xMEI with DEDNPP, strongly supported by the kinetic, NMR and DFT studies. The bottom box shows 2 MEI and 4 MEI, the two species with the lowest reactivity due to the steric hindrance caused by the methyl group, whereas the reactivity difference between 1 MEI and 5 MEI can be attributed to the highest HOMO energy of the latter, as shown in the top box.

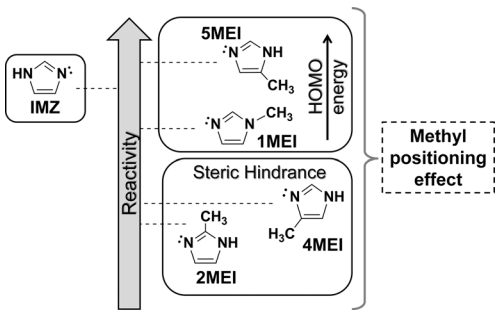

Figure 8. The influence of steric hindrance and HOMO energy caused by the methyl positioning on xMEI reactivity.

In conclusion, we report evidences for the antagonistic methyl positioning effect observed for IMZ derivatives, which shows that both electronic and steric effects contribute to overall behavior. Interestingly, reactivity for the 4(5)MEI tautomers was distinguished and their phosphorylated intermediates were detected by NMR. These results not only fill a gap in the literature with regard to the understanding of mechanistic details, they also provide guidance for designing optimal IMZ-based catalysts for dephosphorylation reactions, with potential applications in detoxification and biological processes.[19] Other substituents on the IMZ ring are being studied, as are some azole drugs.

Experimental Section

Materials

DEDNPP was prepared as described in the literature[4a] and the xMEI derivatives were obtained commercially.

Kinetics

Pseudo first-order conditions were maintained by adding 10 μL of a stock solution of DEDNPP (7.5 mmol L^{-1} in acetonitrile) into 3 mL of a 0.5 mol L^{-1} aqueous solutions of xMEI. The reactions were monitored at 400 nm by means of an UV/Vis spectrophotometer, following the formation of 2,4-dinitrophenoxide (DNP, Scheme 3) and the temperature was controlled with a thermostat-fitted cell holder at 25 °C. The observed first-order rate constants (k_{obs}) were calculated with an iterative least-squares software from the plots of absorbance against time and the correlation coefficients (r) were higher than 0.99 for all curve fittings.

NMR analysis

NMR kinetics were evaluated by adding aliquots of a DEDNPP stock solution (in acetonitrile) to 2 MEI or 4(5)MEI solutions in H_2O, directly into NMR tubes, and then ^1H and ^{31}P NMR spectra were continuous acquired through reaction progress, respectively. Kinetic profiles were obtained by the relative areas of the signals of the $^{31}P\{^1H\}$ NMR spectra that were normalized. The ^1H and $^{31}P\{^1H\}$ NMR spectra were acquired at 298 K in H_2O/acetonitrile (54% *v/v*) containing some D_2O (10% *v/v*) for lock and shimming, on a Bruker AVANCE III 400 NMR spectrometer operating at 9.4 T, observing ^1H and ^{31}P at 400.13 and 161.98 MHz, respectively, equipped with a 5 mm direct detection multinuclear probe with *z*-gradient. One-bond and long-range ^1H–^{13}C and ^1H–^{31}P NMR correlation experiments were acquired on a Bruker AVANCE III 600 NMR spectrometer operating at 14.1 T, observing ^1H, ^{13}C, and ^{31}P at 600.13, 150.90, and 242.94 MHz, respectively, equipped with a 5 mm inverse detection four channel (^1H, ^{13}C, ^{15}N, and ^{31}P) probe with *z*-gradient. ^1H and ^{13}C NMR chemical shifts are given in ppm related to 3-(trimethylsilyl)-2,2′,3,3′-tetradeuteropropionic acid, sodium salt (TMSP-d_4) signal at 0.00 ppm as internal reference, whereas those of ^{31}P NMR are related to H_3PO_4 (85% in D_2O) signal from an external reference.

DFT Calculations

All calculations were performed with Gaussian 09[20] and the water environment was simulated implicitly by the Solvation Model Den-

sity (SMD) method.[21] Geometry optimizations were carried out with the B3LYP[17] and M06–2X[16] functionals combined with 6–31+G(d,p) or 6–311++G(d,p) basis sets. The obtained TS structures presented a single imaginary frequency and no imaginary frequencies were found for minima. To confirm the connectivity of the reaction pathways, IRC[22] calculations were computed with B3LYP/6–31+G(d,p).

Acknowledgements

The authors are grateful to CNPq, CAPES, Finep, L'Oréal-UNESCO-ABC, Fundação Araucária, UFPR, and UTFPR for financial support and fellowships.

Keywords: density functional calculations · imidazole derivatives · kinetics · NMR spectroscopy · tautomer reactivity

[1] a) A. J. Kirby, F. Nome, *Acc. Chem. Res.* **2015**, *48*, 1806–1814; b) F. H. Westheimer, *Science* **1987**, *235*, 1173–1178.
[2] Y. C. Yang, J. A. Baker, J. R. Ward, *Chem. Rev.* **1992**, *92*, 1729–1743.
[3] F. F. Carneiro, W. Pignati, R. M. Rigotto, L. G. S. Augusto, A. Rizollo, N. M. Muller, V. P. Alexandre, K. Friedrich, M. M. S. C. Dossiê, ABRASCO, Um alerta sobre os impactos dos agrotóxicos na saúde, Rio de Janeiro: EPSJV; São Paulo: Expressão Popular, **2015**.
[4] a) E. S. Orth, E. H. Wanderlind, M. Medeiros, P. S. M. Oliveira, B. G. Vaz, M. N. Eberlin, A. J. Kirby, F. Nome, *J. Org. Chem.* **2011**, *76*, 8003–8008; b) P. V. Attwood, M. J. Piggott, X. L. Zu, P. G. Besant, *Amino Acids* **2007**, *32*, 145–156; c) R. T. Raines, *Chem. Rev.* **1998**, *98*, 1045–1065.
[5] L. S. Goodman, A. Gilman, L. L. Brunton, J. S. Lazo, K. L. Parker, Goodman & Gilman's the pharmacological basis of therapeutics, 11th ed., McGraw-Hill, New York, **2006**.
[6] a) E. Capodicasa, P. Cornacchione, B. Natalini, A. Bartoli, S. Coaccioli, P. Marconi, L. Scaringi, *Int. J. Immunopathol. Pharmacol.* **2008**, *21*, 73–85; b) M. Rustia, P. Shubik, *J. Natl. Cancer Inst. (1940-1978)* **1972**, *48*, 721; c) C. E. Voogd, J. J. Vanderstel, J. J. J. A. A. Jacobs, *Mutat. Res.* **1979**, *66*, 207–221.
[7] a) T. C. Bruice, G. L. Schmir, *J. Am. Chem. Soc.* **1957**, *79*, 1663–1667; b) W. P. Jencks, J. Carriuolo, *J. Biol. Chem.* **1959**, *234*, 1272–1279; c) M. Caplow, W. P. Jencks, *Biochemistry* **1962**, *1*, 883; d) J. F. Kirsch, W. P. Jencks, *J. Am. Chem. Soc.* **1964**, *86*, 833; e) J. F. Kirsch, W. P. Jencks, *J. Am. Chem. Soc.* **1964**, *86*, 837; f) Dg. Oakenful, W. P. Jencks, *J. Am. Chem. Soc.* **1971**, *93*, 178; g) H. Neuvonen, *J. Chem. Soc. Perkin Trans. 2* **1987**, 159–167; h) H. Neuvonen, *J. Chem. Soc. Perkin Trans. 2* **1995**, 951–954; i) L. Li, V. S. Lelyveld, N. Prywes, J. W. Szostak, *J. Am. Chem. Soc.* **2016**.
[8] G. S. Li, M. F. RuizLopez, B. Maigret, *J. Phys. Chem. A* **1997**, *101*, 7885–7892.
[9] a) E. S. Orth, T. A. S. Brandao, B. S. Souza, J. R. Pliego, B. G. Vaz, M. N. Eberlin, A. J. Kirby, F. Nome, *J. Am. Chem. Soc.* **2010**, *132*, 8513–8523; b) F. Duarte, J. Aqvist, N. H. Wiliams, S. C. L. Kamerlin, *J. Am. Chem. Soc.* **2015**, *137*, 1081–1093; c) A. J. Kirby, M. Medeiros, J. R. Mora, P. S. M. Oliveira, A. Amer, N. H. Williams, F. Nome, *J. Org. Chem.* **2013**, *78*, 1343–1353.
[10] J. Keeler, P. Wothers, Chemical structure and reactivity : an integrated approach, Oxford University Press, Oxford; New York, **2008**.
[11] B. Lenarcik, P. Ojczenasz, *J. Heterocycl. Chem.* **2002**, *39*, 287–290.
[12] R. B. Campos, E. H. Santos, A. R. M. Oliveira, F. M. M. Ocampos, B. S. Souza, A. Barison, E. S. Orth, *J. Org. Chem.* **2015**, *80*, 7572–7580.
[13] The reversible reaction in the first step is not significant in the overall rate, since it would require DNP to act as a nucleophile regenerating the initial reactant (DEDNPP) and xMEI. This is unfavorable since the pKa of DNP much lower than any xMEI and therefore DNP is a better leaving group. DNP is a poor nucleophile and besides that the pseudo first order conditions in which the experiments were performed make the reverse reaction even more unlikely. It is also corroborated by the drastic consumption of DEDNPP, as shown in the NMR kinetics presented in Figure 4>. Additional data given in SI.
[14] a) H. A. Every, T. A. Zawodzinski, *Electrochemical Society Proceedings* **2004**, *21*, 277–286; b) G. S. Li, M. F. Ruiz-Lopez, M. S. Zhang, B. Maigret, *Theochem. J. Mol. Struct.* **1998**, *422*, 197–204.
[15] J. Shaskus, P. Haake, *J. Org. Chem.* **1983**, *48*, 2036–2038.
[16] Y. Zhao, D. G. Truhlar, *Theor. Chem. Acc.* **2008**, *120*, 215–241.
[17] a) A. D. Becke, *J. Chem. Phys.* **1993**, *98*, 1372–1377; b) P. J. Stephens, F. J. Devlin, C. F. Chabalowski, M. J. Frisch, *J. Phys. Chem.J. Phys. Chem. Us* **1994**, *98*, 11623–11627.
[18] M06–2x optimization calculations with 6-31+G(d,p) and 6–311++G(d,p) were also performed using larger DFT integration (int=ultrafine), nonetheless it still resulted in an inconsistent reactivity trend, compared to experimental data.
[19] a) W. B. Motherwell, M. J. Bingham, Y. Six, *Tetrahedron* **2001**, *57*, 4663–4686; b) K. Kim, O. G. Tsay, D. A. Atwood, D. G. Churchill, *Chem. Rev.* **2011**, *111*, 5345–5403.
[20] M. J. Frisch, G. W. Trucks, H. B. Schlegel, G. E. Scuseria, M. A. Robb, J. R. Cheeseman, G. Scalmani, V. Barone, B. Mennucci, G. A. Petersson, H. Nakatsuji, M. Caricato, X. Li, H. P. Hratchian, A. F. Izmaylov, J. Bloino, G. Zheng, J. L. Sonnenberg, M. Hada, M. Ehara, K. Toyota, R. Fukuda, J. Hasegawa, M. Ishida, T. Nakajima, Y. Honda, O. Kitao, H. Nakai, T. Vreven, J. A. Montgomery Jr., J. E. Peralta, F. Ogliaro, M. J. Bearpark, J. Heyd, E. N. Brothers, K. N. Kudin, V. N. Staroverov, T. Keith, R. Kobayashi, J. Normand, K. Raghavachari, A. P. Rendell, J. C. Burant, S. S. Iyengar, J. Tomasi, M. Cossi, N. Rega, N. J. Millam, M. Klene, J. E. Knox, J. B. Cross, V. Bakken, C. Adamo, J. Jaramillo, R. Gomperts, R. E. Stratmann, O. Yazyev, A. J. Austin, R. Cammi, C. Pomelli, J. W. Ochterski, R. L. Martin, K. Morokuma, V. G. Zakrzewski, G. A. Voth, P. Salvador, J. J. Dannenberg, S. Dapprich, A. D. Daniels, Ö. Farkas, J. B. Foresman, J. V. Ortiz, J. Cioslowski, D. J. Fox, Gaussian, Inc., Wallingford, CT, USA, **2010**.
[21] A. V. Marenich, C. J. Cramer, D. G. Truhlar, *J. Phys. Chem. B* **2009**, *113*, 6378–6396.
[22] K. Fukui, *Acc. Chem. Res.* **1981**, *14*, 363–368.

Received: May 30, 2016
Published online on ■■ ■■, 0000

FULL PAPER

Methyls on the move: The reaction of all monosubstituted methylimidazoles (xMEI) with diethyl 2,4-dinitrophenyl phosphate has been evaluated by kinetics studies, nuclear magnetic resonance analysis and DFT calculations (see figure). The electron-donating methyl group acts to decrease the reactivity of the xMEI, except for 4(5)methylimidazole. This behavior was attributed to both electronic and steric effects. The tautomer reactivity was distinguished.

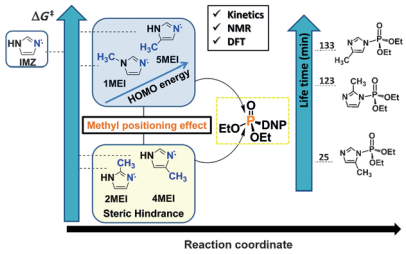

Tautomer Reactivity

*R. B. Campos, L. R. A. Menezes, A. Barison, D. J. Tantillo, E. S. Orth**

■■ – ■■

The Importance of Methyl Positioning and Tautomeric Equilibria for Imidazole Nucleophilicity